Crystal structure of an aromatic ring opening dioxygenase LigAB, a protocatechuate 4,5-dioxygenase, under aerobic conditions

Keisuke Sugimoto[1], Toshiya Senda[1]*, Hisae Aoshima[2], Eiji Masai[2], Masao Fukuda[2] and Yukio Mitsui[1]*

Background: *Sphingomonas paucimobilis* SYK-6 utilizes an extradiol-type catecholic dioxygenase, the LigAB enzyme (a protocatechuate 4,5-dioxygenase), to oxidize protocatechuate (or 3,4-dihydroxybenzoic acid, PCA). The enzyme belongs to the family of class III extradiol-type catecholic dioxygenases catalyzing the ring-opening reaction of protocatechuate and related compounds. The primary structure of LigAB suggests that the enzyme has no evolutionary relationship with the family of class II extradiol-type catecholic dioxygenases. Both the class II and class III enzymes utilize a non-heme ferrous center for adding dioxygen to the substrate. By elucidating the structure of LigAB, we aimed to provide a structural basis for discussing the function of class III enzymes.

Results: The crystal structure of substrate-free LigAB was solved at 2.2 Å resolution. The molecule is an $\alpha_2\beta_2$ tetramer. The active site contains a non-heme iron coordinated by His12, His61, Glu242, and a water molecule located in a deep cleft of the β subunit, which is covered by the α subunit. Because of the apparent oxidation of the Fe ion into the nonphysiological Fe(III) state, we could also solve the structure of LigAB complexed with a substrate, PCA. The iron coordination sphere in this complex is a distorted tetragonal bipyramid with one ligand missing, which is presumed to be the O_2-binding site.

Conclusions: The structure of LigAB is completely different from those of the class II extradiol-type dioxygenases exemplified by the BphC enzyme, a 2,3-dihydroxybiphenyl 1,2-dioxygenase from a *Pseudomonas* species. Thus, as already implicated by the primary structures, no evolutionary relationship exists between the class II and III enzymes. However, the two classes of enzymes share many geometrical characteristics with respect to the nature of the iron coordination sphere and the position of a putative catalytic base, strongly suggesting a common catalytic mechanism.

Addresses: [1]Division of Protein Engineering, Department of BioEngineering, Nagaoka University of Technology, Nagaoka, Niigata 940-2188, Japan and [2]Division of Microbial Engineering, Department of BioEngineering, Nagaoka University of Technology, Nagaoka, Niigata 940-2188, Japan.

*Corresponding authors.
E-mail: mitsui@vos.nagaokaut.ac.jp
senda@vos.nagaokaut.ac.jp

Key words: extradiol-type dioxygenase, lignin degradation, metalloprotein, mononuclear iron, ring-opening enzyme

Received: 18 January 1999
Revisions requested: 25 February 1999
Revisions received: 23 March 1999
Accepted: 15 April 1999

Published: 20 July 1999

Structure August 1999, 7:953–965
http://biomednet.com/elecref/0969212600700953

 ISSN 0969-2126

Introduction

Aromatic compounds derived from natural and industrial sources permeate the biosphere. Their sheer abundance makes them worthy targets as bacterial carbon sources, and the most prevalent are readily metabolized, chiefly by aerobic strains via oxidative pathways [1]. The compounds most frequently found at the confluence of aromatic degradation pathways of aerobic bacteria include catechol, protocatechuate (PCA), gentisate, gallate and their analogs. The reaction catalyzed by the ring-opening enzymes metabolizing these compounds is the most significant single step in the bacterial assimilation of aromatics [2]. In aerobic bacteria, catechol and other dioxygenases almost exclusively catalyze the reactions of aromatic ring fission.

On the basis of the type of reaction catalyzed, the ring-opening catecholic dioxygenases can be classified into two types, the intradiol type and the extradiol type [1]. It has been established that the intradiol-type (catecholic) dioxygenases have non-heme-type ferric iron in their active site, whereas extradiol-type (catecholic) dioxygenases typically have non-heme-type ferrous iron in their active site [1]. The distinct oxidation state of the iron in the active site between intradiol- and extradiol-type dioxygenases leads to a distinct product, even if they exert the catalytic reaction on the same substrate. The extradiol-type dioxygenases catalyze the ring-cleavage at the C–C bond adjacent to the vicinal hydroxyl groups, whereas the intradiol-type dioxygenases cleave the C–C bond between the vicinal hydroxyl groups. The detailed reaction mechanism of the intradiol-type dioxygenase has been analyzed extensively using crystallographic, spectroscopic and other methods [3–8]. The details of the catalytic mechanism of the extradiol-type dioxygenases, however, are not yet well understood.

To date three classes of extradiol-type (catecholic) dioxygenases have been identified, class I, II and III [9]. Comparisons of the primary structures between class I and II enzymes have revealed that the two kinds of enzymes have a common ancestor, the class II enzymes having evolved from a class I enzyme through gene duplication [9,10]. As a result, the class II enzymes are composed of two domains with approximately the same folding pattern as each other [11–13]. To date, several crystal structures of the class II extradiol-type dioxygenases have been determined by other groups and ourselves [11–14]. Among these, we first solved the structure of BphC, a 2,3-dihydroxybiphenyl 1,2-dioxygenase from a *Pseudomonas* species [11]. Subsequently, we prepared various mutant proteins of BphC and determined their crystal structures [15]. Analyzing these crystal structures as well as their kinetic parameters, we obtained the following results. First, two hydroxyl groups of the substrate directly coordinate to the Fe ion with trigonal bipyramidal geometry [11,12]. The coordination geometry suggests that the hydroxyl group on the equatorial plane is deprotonated, whereas the hydroxyl group in the axial position is not [15]. This feature of the asymmetric deprotonation is consistent with the previously proposed reaction mechanism [16,17]. Second, the precisely complementary surface shape between the substrate and its binding pocket, rather than the coordination between the Fe ion and the two hydroxyl groups of the substrate, seems to be the dominant factor in stabilizing substrate binding [15]. Third, His194 is indispensable for the catalysis of BphC [12,15]; it most probably acts as a base in the catalysis. The presence of such a base catalyst has been predicted by spectroscopic analyses [16]. Because of the primary structural similarity, these results seem to extend to other extradiol-type dioxygenases belonging to classes I and II.

Figure 1

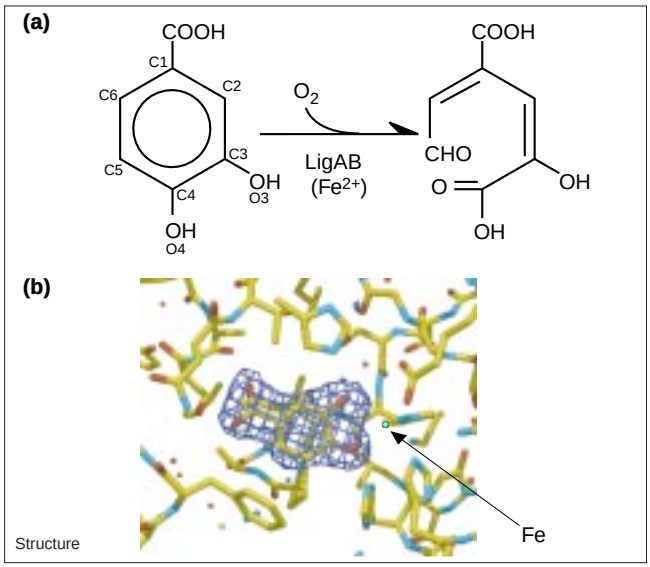

Degradation of the bound substrate, PCA, by LigAB. (a) The enzymatic reaction catalyzed by LigAB. A ferrous ion and a dioxygen are required. The numbering scheme for the protocatechuate ring is indicated. (b) Omit map for bound PCA, colored blue, in the LigAB–PCA complex. The Fe ion is in green. (The figure was prepared using the programs XtalView [34] and Raster3D [35].)

The amino acid sequence similarity between the class I and II extradiol-type (catecholic) dioxygenases is apparent, as described above, but the amino acid sequences of the class III dioxygenases do not show any similarities to these common sequences [10]. Spectroscopic studies, however, have suggested that the class III enzymes share several common active-site characteristics with the class II enzymes [18–20]. Details of the catalytic mechanism of the class III extradiol-type (catecholic) dioxygenases, however, have not been well understood because of a total lack of three-dimensional (3D) structural information for this type of enzyme. An electron paramagnetic resonance (EPR) study with a ^{17}O-labeled substrate [20] indicated that the hydroxyl groups of the substrate directly coordinate to the ferrous iron in the active site. On the basis of these results, some models of the coordination system for a ferrous iron in the active site have been proposed [20]. In the absence of crystallographic information, however, no sound discussion as to the enzymatic reaction mechanism has been possible. Thus, knowledge of the 3D structures of the class III enzymes has long been awaited.

Here, we report the crystal structure of a class III extradiol-type catecholic dioxygenase, LigAB, which is a protocatechuate 4,5-dioxygenase. To the best of our knowledge, this is the first report on the 3D structure of a dioxygenase in this class. We find that the overall structure of LigAB is completely different from that of BphC and other type II extradiol-type (catecholic) dioxygenases, and infer that no evolutionary relationship exists between the class II and III enzymes. The coordination sphere of LigAB, however, exhibits several characteristics common to BphC. Moreover, the disposition of the putative catalytic base is very similar between the two enzymes. These results strongly suggest that the class II and III enzymes share a common catalytic mechanism despite their completely different 3D structures. Thus, this seems to be an example of convergent evolution of two proteins that have no overall sequence and structural similarity with each other.

The LigAB enzyme, which is derived from *Sphingomonas paucimobilis* SYK-6 [21], has an $\alpha_2\beta_2$ subunit composition and contains a ferrous iron in the active site (HA, EM, MF, unpublished results). This enzyme catalyzes a ring-opening reaction of PCA, as shown in Figure 1a. Therefore, LigAB is enzymologically classified as a protocatechuate 4,5-dioxygenase. LigAB has been identified as a key enzyme in the lignin-degradation pathway of *S. paucimobilis* SYK-6 [21]. A

variety of aromatics derived from lignin are metabolized via formation of PCA in this strain.

Finally, one reservation has to be made as to the relevance of the structures presented here to the active site of the enzyme. As all the experiments presented here were performed under aerobic conditions, the Fe ions were most probably oxidized to the non-physiological Fe(III) (ferric) state. And this is perhaps the reason why we could observe the enzyme complexed with an intact substrate. For this reason, any conclusions drawn about the reaction mechanism using our structure should be treated with caution; this discussion should be based on fine details of the active-site structure.

Results and discussion

Structure determination

The crystal structure of LigAB was determined at 2.2 Å resolution by multiple isomorphous replacement (MIR) methods (Table 1). Density modification was combined with noncrystallographic-symmetry averaging to improve the quality of the MIR electron-density map. On the basis of the map, we could readily build the model for the $\alpha_2\beta_2$ assembly (860 amino acids in total) into the density. The protein structure was refined until convergence of the refinement was reached, resulting in an R factor of 16.0% (Table 1).

The structure of LigAB in complex with PCA (hereafter, the LigAB–PCA complex) was also determined at 2.2 Å resolution (Table 1). The crystals of LigAB–PCA were prepared by the soaking method. As the crystals were isomorphous with those of the substrate-free form, the difference Fourier method was applied to obtain the electron density for PCA. The density located just beside the Fe ion clearly indicated an uncleaved PCA molecule, as seen in Figure 1b.

Thus, the LigAB enzyme in our crystals must have been inactivated as a result of the oxidation of Fe into the ferric form. Indeed, the enzyme dissolved from these crystals showed no activity but it was restored upon addition of ferrous iron or ascorbate. One possible counter argument against this notion is the color of the crystals. They were light yellow rather than dark red, which is said to be characteristic of the charge-transfer complex between a ferric iron and bound catecholic substrate. The thinness of the crystals (less than 0.1 mm) might explain this.

Quaternary structure

On the basis of a gel-filtration column chromatography analysis, LigAB was shown to have an $\alpha_2\beta_2$ subunit composition (HA, unpublished results). Crystallographic results confirmed the $\alpha_2\beta_2$ subunit composition, which appeared as a compact assembly (Figure 2a). When specifying an amino acid residue of the α subunit, we will attach the suffix 'a' to the residue, for example, Tyr90a. Similarly, for the β subunit, suffix 'b' will be attached. Subunits related by the noncrystallographic twofold axis are distinguished by suffixes 1 and 2 (for example, α1, β1, α2 and β2) when needed.

Table 1

Data collection and structure determination statistics for LigAB.

Data set	Native*	Mersalyl acid	$K_2Au(CN)_2$	PCA complex
Data collection				
Resolution (Å)	60–2.2	40–2.5	60–2.5	60–2.2
Unique reflections/observed reflections	43,335/80,490	33,528/124,528	33,771/94,187	45,587/91,377
Completeness (%)	86.5	93.7	94.9	91.0
$< I >/< \sigma I >$	9.8	15.3	8.5	11.0
R_{merge} (%)	4.75	3.9	5.8	5.45
MIR phasing (60–2.5 Å)				
R_{iso} (%)		17.0	10.2	
R_{Cullis}		0.63	0.85	
Phasing power		1.00	0.55	
Mean figure of merit (acentric/centric)		0.38 (0.37/0.59)		
Refinement (60–2.2 Å)				
Reflections used ($F > 1\sigma$)	43,259			45,584
Number of protein atoms	6688			6688
Number of ligand atoms	0			22
Number of water atoms	200			189
R factor (%)	16.0			16.1
R_{free}†(%)	21.6			22.0
Rms deviation from ideality				
bonds (Å)	0.016			0.016
angles (Å)	2.1			2.0

*Space group $P2_1$: *a* = 65.4 Å, *b* = 66.5 Å, *c* = 119.8 Å, β = 92.5°. †R_{free} was calculated using a subset (10%) of the data.

Figure 2

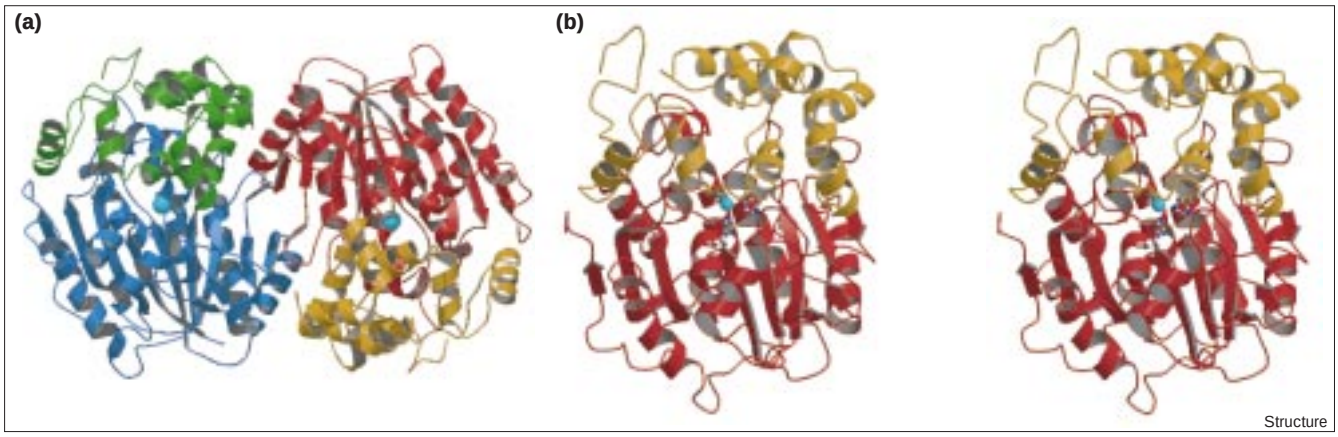

Overall structure of LigAB. **(a)** An $\alpha_2\beta_2$ tetramer viewed along a noncrystallographic twofold axis. The β subunits (related by the twofold axis) are colored red and blue, and the α subunits are colored orange and green. The Fe ion is shown as a cyan sphere. **(b)** An αβ protomer colored as in (a); the view direction is approximately horizontal to that in (a). Three amino acid residues coordinated to the Fe ion are shown in ball-and-stick representation. (These figures were prepared using the programs MOLSCRIPT [36] and Raster3D [35].)

The $\alpha_2\beta_2$ assembly of LigAB is shown in Figure 2a. It has approximate dimensions of $75 \times 50 \times 50$ Å^3. In the tetrameric molecule, the two β subunits, which are related by a noncrystallographic twofold axis, make direct contacts with a buried surface area of 1971 Å^2. The two α subunits do not make direct contacts. Instead each of them makes extensive contacts with a partner β subunit, with a buried surface area of 3552 Å^2. Thus, the molecule can be

Figure 3

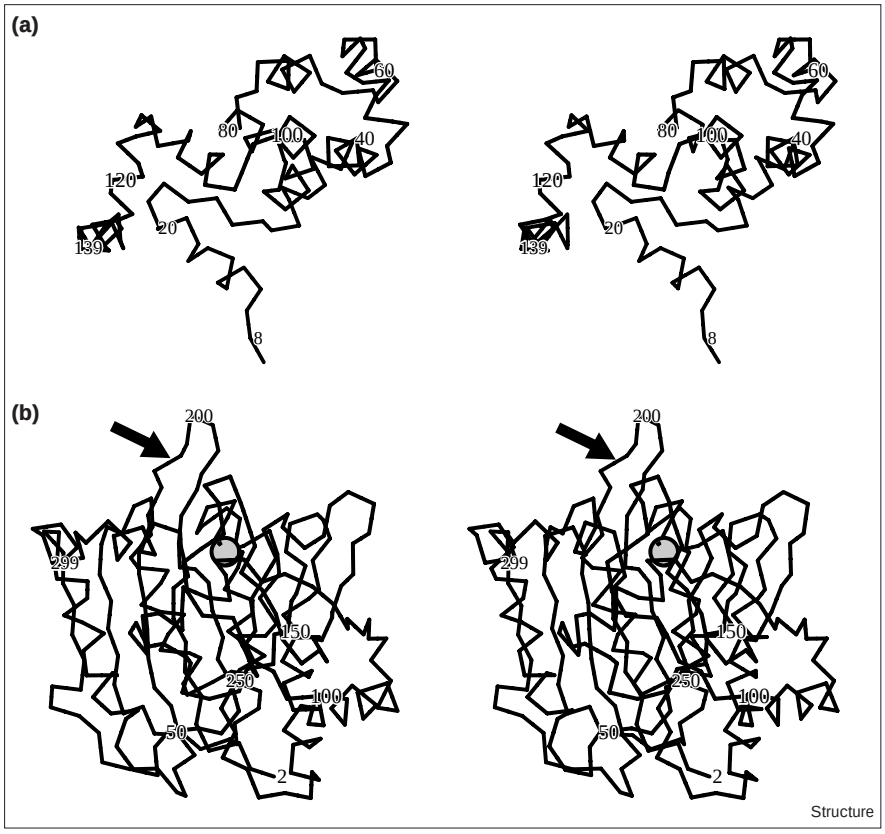

Stereoview Cα trace of **(a)** the α subunit and **(b)** the β subunit. The Fe ion in the β subunit is shown as a shaded sphere. The arrow indicates the site of insertion of a long loop in some of the class III dioxygenases (see text). (These figures were prepared using the program MOLSCRIPT [36].)

described as a relatively loose dimer of two tightly bound α–β heterodimers.

Structure of the α and β subunits

The α subunit is a small subunit composed of 139 amino acid residues. It has a plate-like shape with approximate dimensions of 50 × 40 × 15 Å^3 (Figure 3a). The subunit is composed of ten α helices, which are designated α1–α10, as shown in Figure 4a. Residues 35a–109a form a relatively compact structure whereas the remaining parts of the molecule are rather isolated, resulting in a large surface area of the α subunit that contributes to the extensive interaction between the α and β subunits. Residues 85a–110a cover the active-site pocket that is located in the β subunit.

The β subunit is large, being composed of 302 amino acid residues. This subunit is roughly spherical with approximate dimensions of 50 × 40 × 40 Å^3 (Figure 3b). The β submit seems to have an α/β structure composed of 11 β strands, nine α helices and one 3_{10} helix. These secondary structural elements are designated as shown in Figure 4b. The β sheet located in the central core of the subunit consists of nine β strands, six of which are arranged in a parallel manner, with the others arranged in an antiparallel manner. The β-subunit structure seems to have a novel type of folding because a database search using SCOP [22] could not detect any structure with the same folding pattern.

Despite the speculation by Spence *et al.* [9], the β subunit seems to be a single entity with no sign of division into domain structure (Figure 2b). Important amino acid residues in the active site are contributed from all portions of the polypeptide chain (Figures 4b). Upon re-examination of the sequence alignment of the N-terminal and C-terminal 'halves' [9] we see a slight similarity between them in only the first one-sixth portion of the 'half'. This situation, which is most probably a general feature of class III enzymes, is in sharp contrast to the situation with the polypeptide chains of class II enzymes such as BphC where evidence for a gene duplication is abundant, the 3D structure is clearly composed of two domains, and the single active site is exclusively composed of amino acid residues from the C-terminal domain [12].

The iron coordination sphere in the substrate-free form

The active site is located at the bottom of the deep cleft that is found in the upper part of the β subunit (Figure 3b). Moreover, the otherwise exposed cleft is extensively covered by the partner α subunit. Thus, the Fe ion in the active site is well buried, being located ~15 Å below the surface of the α–β heterodimer. In the substrate-free form, the Fe ion is directly coordinated by His12b (N–Fe, 2.0 Å), His61b (N–Fe, 2.1 Å) and Glu242b (O–Fe, 2.0 Å) (Figure 5a). In addition, one water molecule can be assigned at a distance of 1.8 Å from the iron center (Figure 5a,c). (The distances given in the figure and the above text are the values averaged over the two subunits. For individual values, see Table 2.) The coordination sphere can be described as a distorted trigonal pyramid with the water molecule in the axial position and the three proteinaceous ligands in equatorial positions (Figure 5a).

Figure 4

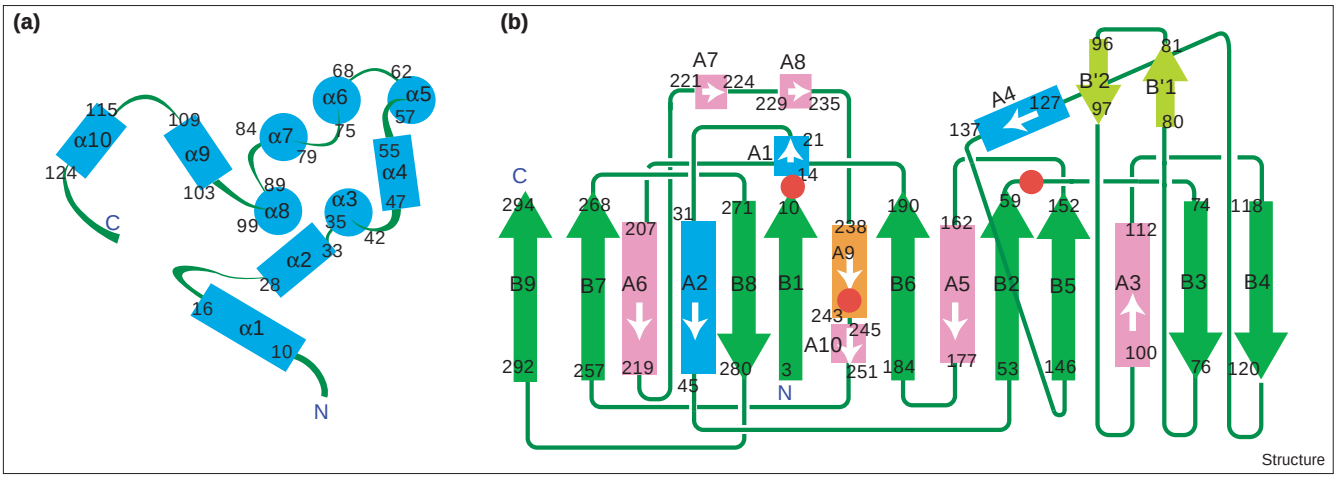

Chain-folding topologies in **(a)** the α subunit, and **(b)** the β subunit. In (a), α helices running approximately perpendicular and parallel to the paper are depicted by circles and rectangles, respectively. In (b), β strands are depicted as arrows, while α helices and the 3_{10} helix (A9, in orange) are depicted as rectangles with the inside arrows indicating the chain direction. The nine β strands shown in green form a core β sheet, which is sandwiched by the six α helices shown in pink from one side (the far side in Figure 3b) and by three α helices shown in blue from the other side (the front side in Figure 3b). β Strands that do not constitute the core β sheet are colored light green, and separately designated with a prime, B′1 and B′2. The amino acid residues coordinating the Fe ion in the active site are indicated by red circles.

Figure 5

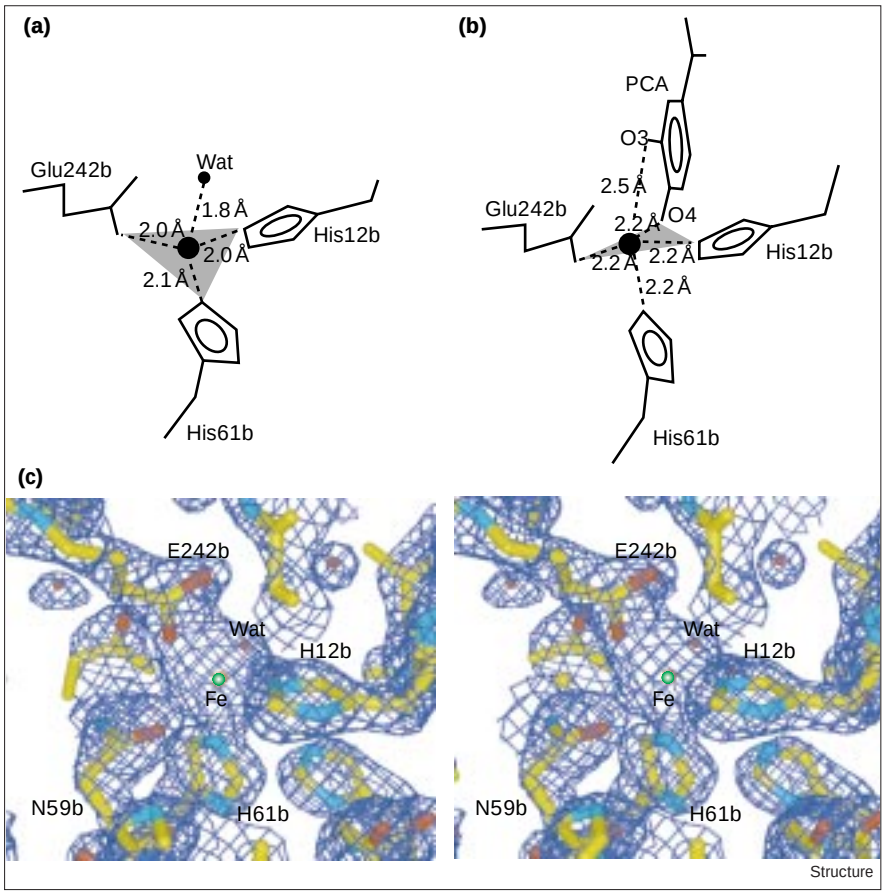

Geometries of the iron coordination spheres in (a) substrate-free LigAB and (b) the LigAB–PCA complex. The distances are averaged over the β1 and β2 subunits. (c) $2F_o–F_c$ electron-density map corresponding to (a). The Fe ion is shown in green. (Part (c) was prepared using the programs XtalView [34] and Raster3D [35].)

The iron atom is located 0.5 Å above the plane formed by the equatorial ligands. In addition to the four ligands described above, Oδ of Asn59 makes a weak interaction with the Fe ion at a distance of 2.9 Å from the opposite side of the equatorial plane (Figure 5c).

The three amino acid residues coordinated to the Fe ion are completely conserved among the related enzymes (Figure 6), most probably reflecting the similar coordination geometries shared by them. The weak ligand Asn59b, however, seems to be unique to LigAB as it is highly variable in the related enzymes. Among the three conserved ligands, the positions of His12b and His61b seems to be relatively flexible — they are located on loop regions immediately following the β strands (the B1 strand and B2 strand, respectively), whereas the position of Glu242b, being fixed to the A9 3_{10} helix, seems to be relatively inflexible. The relative flexibility mentioned above seems to allow a conformational change of the coordination sphere upon binding the substrate (see below). Here it should be recalled that, in the case of BphC [12], all the residues coordinated to the Fe ion were fixed on the β strands [12], providing a rigid framework for the coordination sphere. Seemingly due to this structural characteristic, the BphC enzyme does not show prominent induced-fit movements upon binding a substrate [12].

The iron coordination sphere in the LigAB–PCA complex

The coordination sphere found in the LigAB–PCA complex is shown in Figure 5b. In the present interpretation, the two hydroxyl groups of the substrate, PCA, directly coordinate to the Fe ion as predicted by an EPR study on protocatechuate 4,5-dioxygenase using the ^{17}O-labeled substrate [20]. The coordination sphere can be described as a distorted tetragonal bipyramid with His12b, Glu242b and O4 of PCA being the equatorial ligands and His61b and O3 of PCA being the axial ligands. One site among the four potential sites in the equatorial plane seems to be unliganded. As described below, we speculate that this missing site is the binding site for a dioxygen needed for the catalytic reaction (Figure 7a). A group of water molecules bound to the Fe ion in the substrate-free form were displaced by bound PCA, as predicted by Arciero *et al.* [20]. Somehow the distances between the Fe ion and proteinaceous ligands

are slightly larger than those found in the substrate-free form (compare the values given in Figure 5b with those given in Figure 5a).

The binding pocket for PCA as an intersubunit closed cavity

The substrate, PCA, is accommodated in a cavity located in the upper part of the β subunit (Figure 3b). The cavity is ~5 Å deep and lined by four loops (residues 11–15, 58–62, 153–156 and 191–197), two helices (126–131 and 238–243) and one β strand (270–273). Helices α8 and α9 from the α subunit form a lid that closes the open end of the pocket. Consequently, the bound substrate PCA is completely inaccessible from the solvent. This feature of complete containment seems to be essential for the activity of this class of enzymes. Thus, in some of the related enzymes such as MpcI (Figure 6), which lacks the α subunit, a long insertion of 42–44 residues is commonly observed between residues 203 and 204 (LigAB numbering). As the insertion point is located close to one of the side walls of the PCA-binding pocket of the β subunit (indicated by an arrow in Figure 3b), the long insertion segment must be folded and situated on top of the pocket to mimic the role of the α subunit in LigAB. In the absence of the substrate, the closed substrate cavity formed at the interface is occupied by five trapped water molecules.

The complementation between the van der Waals surface of bound PCA and the inner van der Waals surface of the closed cavity is very good. More specifically, the aromatic ring of PCA makes contacts with a group of hydrophobic residues, Ile13b, Pro14b, Leu197b, Phe103a, His195b and Thr271b (Figure 7a). It is noteworthy that C5 of PCA, which is the site of attack by an activated dioxygen [20], has no access at all to the outside solvent space. The most direct obstacle to this access is Phe103a from the α subunit. Thus, a rather large-scale dynamic motion inside the subunits and a relative motion between the two subunits must be required for reaction.

In addition to the above-mentioned nonspecific van der Waals interactions between the substrate and the enzyme cavity, several coordination and hydrogen-bond interactions between them determine the orientation of PCA. Thus, O3 and O4 are hydrogen bonded to Nε of His195b and Nε of His127b, respectively, in addition to their coordination to the Fe ion. The O3 atom also participates in another bifurcated hydrogen bond to a bound water molecule that, in turn, is hydrogen bonded to Oγ of Ser11b. Of the two carboxylate oxygens of PCA, one makes a hydrogen bond to the mainchain N of Asn270b and the other makes a set of bifurcated hydrogen bonds to Oγ of Ser269b and Nδ of Asn270b (Figure 7a). The negative charge associated with the PCA carboxylate may well be compensated for by the virtual negative charge provided by helices α9 and A1.

Table 2

Geometrical details of the Fe coordination spheres.

Subunit	β1	β2	Average
Substrate-free form			
Bond distances (Å)			
Fe–His12b Nε	2.1	1.9	2.0
Fe–His61b Nε	2.1	2.0	2.1
Fe–Glu242b Oε	1.9	2.0	2.0
Fe–Wat	1.7	1.8	1.8
Fe–Thr59b Oγ	3.0	2.8	2.9
Bond angles (°)			
His12b Nε–Fe–His61b Nε	104.0	109.8	106.9
His61b Nε–Fe–Glu242b Oε	125.3	125.5	125.4
Glu242b Oε–Fe–His12b Nε	124.8	121.6	123.2
His12b Nε–Fe–Wat	102.6	106.1	104.4
His61b Nε–Fe–Wat	101.8	96.1	99.0
Glu242b Oε–Fe–Wat	91.2	86.4	88.8
PCA complex			
Bond distances (Å)			
Fe–His12b Nε	2.2	2.2	2.2
Fe–His61b Nε	2.3	2.1	2.2
Fe–Glu242b Oε	2.1	2.2	2.2
Fe–PCA O3	2.4	2.5	2.5
Fe–PCA O4	2.2	2.1	2.2
His195 Nε–PCA O3	2.9	2.9	2.9
His127 Nε–PCA O4	2.5	2.6	2.6
Bond angles (°)			
His12b Nε–Fe–PCA O4	110.0	112.9	111.5
PCA O4–Fe–Glu242b Oε	143.4	142.8	143.1
Glu242b Oε –Fe–His12b Nε	106.4	104.3	105.4
His12b Nε–Fe–PCA O3	98.6	98.4	98.5
PCA O4–Fe–PCA O3	72.3	77.5	74.9
Glu242b Oε–Fe–PCA O3	105.4	97.8	101.6
His12b Nε–Fe–His61b Nε	85.1	87.5	86.3
His61b Nε–Fe–His61b Nε	87.1	83.1	85.1
Glu242b Oε–Fe–His61b Nε	93.0	98.7	95.9

The presence of a carboxylate group at C1 of the substrate seems to be essential for the catalysis by LigAB. Thus, LigAB shows little activity for catechol and its derivatives lacking the carboxylate group (HA, unpublished results). Indeed, structural analysis using a crystal soaked in the standard buffer containing 10 mM catechol exhibited no clear electron density for catechol. Thus, the carboxylate group must play the role of anchor for the substrate via van der Waals interactions and a set of hydrogen bonds with the surrounding protein groups. It is noteworthy that the mere existence of two hydroxyl groups, despite their strong interaction with the surrounding protein atoms via both the Fe coordination and hydrogen-bond interactions, is not sufficient for catalysis to proceed. The above observation has also been made by Arciero *et al.* [20] on the basis of spectroscopic studies.

The coordination mode of the substrate PCA to the Fe ion

Of the two hydroxyl oxygens of PCA, O3 and O4 are, respectively, axially and equatorially coordinated to Fe (Figure 5b). As the precise Fe–O distance is critical for

Figure 6

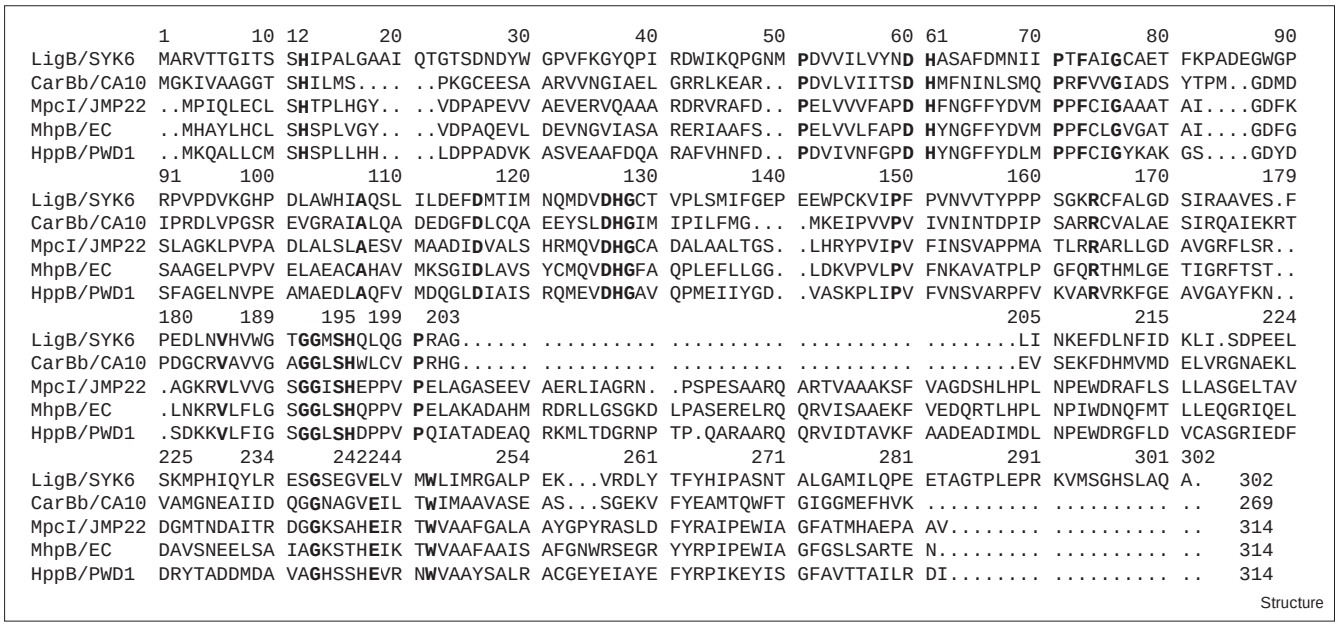

```
           1       10 12      20         30         40         50         60 61      70         80         90
LigB/SYK6  MARVTTGITS SHIPALGAAI QTGTSDNDYW GPVFKGYQPI RDWIKQPGNM PDVVILVYND HASAFDMNII PTFAIGCAET FKPADEGWGP
CarBb/CA10 MGKIVAAGGT SHILMS.... ..PKGCEESA ARVVNGIAEL GRRLKEAR.. PDVLVIITSD HMFNINLSMQ PRFVVGIADS YTPM..GDMD
MpcI/JMP22 ..MPIQLECL SHTPLHGY.. ..VDPAPEVV AEVERVQAAA RDRVRAFD.. PELVVVFAPD HFNGFFYDVM PPFCIGAAAT AI....GDFK
MhpB/EC    ..MHAYLHCL SHSPLVGY.. ..VDPAQEVL DEVNGVIASA RERIAAFS.. PELVVLFAPD HYNGFFYDVM PPFCLGVGAT AI....GDFG
HppB/PWD1  ..MKQALLCM SHSPLLHH.. ..LDPPADVK ASVEAAFDQA RAFVHNFD.. PDVIVNFGPD HYNGFFYDLM PPFCIGYKAK GS....GDYD
           91     100        110        120        130        140        150        160        170        179
LigB/SYK6  RPVPDVKGHP DLAWHIAQSL ILDEFDMTIM NQMDVDHGCT VPLSMIFGEP EEWPCKVIPF PVNVVTYPPP SGKRCFALGD SIRAAVES.F
CarBb/CA10 IPRDLVPGSR EVGRAIALQA DEDGFDLCQA EEYSLDHGIM IPILFMG... .MKEIPVVPV IVNINTDPIP SARRCVALAE SIRQAIEKRT
MpcI/JMP22 SLAGKLPVPA DLALSLAESV MAADIDVALS HRMQVDHGCA DALAALTGS. .LHRYPVIPV FINSVAPPMA TLRRARLLGD AVGRFLSR..
MhpB/EC    SAAGELPVPV ELAEACAHAV MKSGIDLAVS YCMQVDHGFA QPLEFLLGG. .LDKVPVLPV FNKAVATPLP GFQRTHMLGE TIGRFTST..
HppB/PWD1  SFAGELNVPE AMAEDLAQFV MDQGLDIAIS RQMEVDHGAV QPMEIIYGD. .VASKPLIPV FVNSVARPFV KVARVRKFGE AVGAYFKN..
           180    189    195 199  203                                                  205        215        224
LigB/SYK6  PEDLNVHVWG TGGMSHQLQG PRAG..... ..........  ..........  ..........  ........LI NKEFDLNFID KLI.SDPEEL
CarBb/CA10 PDGCRVAVVG AGGLSHWLCV PRHG..... ..........  ..........  ..........  ........EV SEKFDHMVMD ELVRGNAEKL
MpcI/JMP22 .AGKRVLVVG SGGISHEPPV PELAGASEEV AERLIAGRN. .PSPESAARQ ARTVAAAKSF VAGDSHLHPL NPEWDRAFLS LLASGELTAV
MhpB/EC    .LNKRVLFLG SGGLSHQPPV PELAKADAHM RDRLLGSGKD LPASERELRQ QRVISAAEKF VEDQRTLHPL NPIWDNQFMT LLEQGRIQEL
HppB/PWD1  .SDKKVLFIG SGGLSHDPPV PQIATADEAQ RKMLTDGRNP TP.QARAARQ QRVIDTAVKF AADEADIMDL NPEWDRGFLD VCASGRIEDF
           225    234     242244        254        261        271        281        291        301 302
LigB/SYK6  SKMPHIQYLR ESGSEGVELV MWLIMRGALP EK...VRDLY TFYHIPASNT ALGAMILQPE ETAGTPLEPR KVMSGHSLAQ A.   302
CarBb/CA10 VAMGNEAIID QGGNAGVEIL TWIMAAVASE AS...SGEKV FYEAMTQWFT GIGGMEFHVK ..........  ..........  ..   269
MpcI/JMP22 DGMTNDAITR DGGKSAHEIR TWVAAFGALA AYGPYRASLD FYRAIPEWIA GFATMHAEPA AV........  ..........  ..   314
MhpB/EC    DAVSNEELSA IAGKSTHEIK TWVAAFAAIS AFGNWRSEGR YYRPIPEWIA GFGSLSARTE N.........  ..........  ..   314
HppB/PWD1  DRYTADDMDA VAGHSSHEVR NWVAAYSALR ACGEYEIAYE FYRPIKEYIS GFAVTTAILR DI........  ..........  ..   314
```

Structure

Amino acid sequence alignment of some of the class III dioxygenases. For the upper two enzymes, only the sequences for the β subunit (LigB, CarBb) are shown. For the lower three enzymes, the subunit corresponding to the α subunit of LigAB does not exist. The conserved amino acid residues are shown in bold typeface. The sequences aligned are as follows (references and GenBank accession numbers are given in parentheses): LigB/SYK6, *Sphingomonas paucimobilis* SYK-6 protocatechuate 4,5-dioxygenase (β subunit) [21] (M34835); CarBb/CA10, *Pseudomonas* sp. strain CA10 carbazole 1,9a-dioxygenase (β subunit) [37] (D89064); MpcI/JMP22, *Alcaligenes eutrophus* JMP222 catechol 2,3–dioxygenase I [38] (X52414); MhpB/EC, *Escherichia coli* catechol 2,3-dioxygenase [9] (D86239); HppB/PWD1, *Rhodococcus globerulus* PWD1 2,3-dihydroxylphenyl-propionate 1,2-dioxygenase [39] (U89712).

judging whether the oxygen is in the hydroxyl or oxyanion state, which, in turn, is critical for mechanistic discussion, we carried out relevant refinement procedures very carefully. Within the allowable limit of the electron density for PCA in the $2F_o–F_c$ map, we tried various positions and orientations of PCA as starting points. The artificial restraints to force equivalent geometry onto the crystallographically independent β1 and β2 subunits (noncrystallographic-symmetry restraints) were deliberately removed. As shown in Table 2, the resultant distances (values for β1, β2 subunits in parentheses) are commonly shorter for equatorial Fe–O4 (2.2 Å, 2.1 Å) and longer for axial Fe–O3 (2.4 Å, 2.5 Å). Considering the error in coordinates (0.23 Å) estimated from a Luzzati plot [23], the equatorial distances are only marginally significantly shorter than the axial distances. In the model compound in which 3,5-di-*tert*-butylcatechol is coordinated to Fe(II), the hydroxy oxygen and oxyanion are coordinated with the distances of 2.263 Å and 1.953 Å, respectively [16]. Thus it is likely that O4 is in the anionic state whereas O3 is in the hydroxyl state. It is intriguing to note that the asymmetric binding in this mode is consistent with the proposed reaction mechanism [16,17]. However, in this mechanism the presence of Fe(II) rather than Fe(III) (as in the crystals used in this study) is essential. As for the charge balance around Fe, presence of a carboxylate from Glu242b and an oxyanion from the catecholic ring would compensate the positive charge provided by Fe(II) but not Fe(III). Despite these ambiguities and inconsistencies, we feel it rather likely that the topological nature (the manner of ligand arrangement) of the Fe sphere remains the same even in the physiological Fe(II) state, as the substrate PCA and the surrounding amino acid residues seem to be restrained by so many interactions, as described in the preceding sections. The details of the geometry and electrostatics, however, may well be different, especially in view of the observed induced-fit movements described below. Thus, the details will be established only by relevant crystallographic and other experiments being carried out under anaerobic conditions.

Induced-fit movements upon substrate binding

Upon binding the substrate PCA, the active site of LigAB in the present structure is affected by a set of rather conspicuous induced-fit movements. Referring to Figure 8a, these movements may be described as follows. His13b and Pro14b shift rightward to accommodate the PCA molecule, the adjacent residue His12b is lifted concomitantly. Apparently related to this movement, the Fe ion is lifted by ~1.4 Å. The lifted Fe position is suitable for coordination

Figure 7

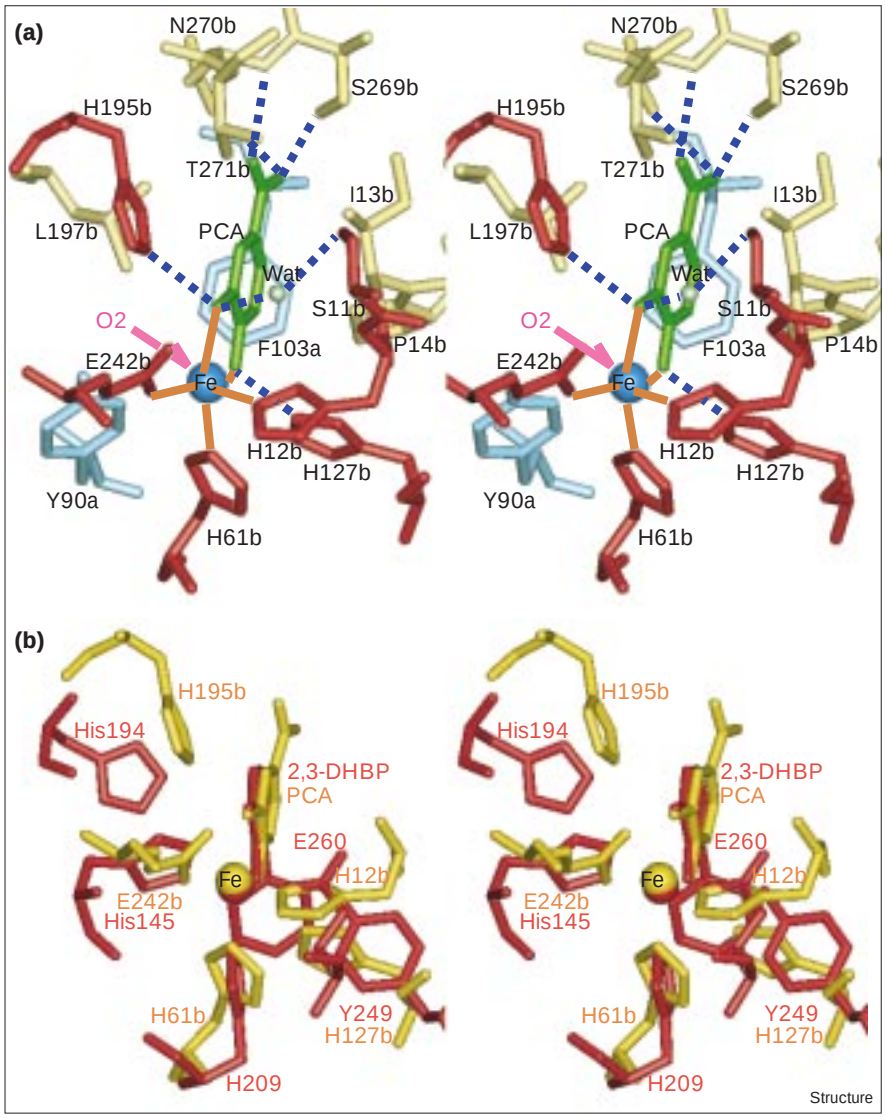

The active site of the LigAB–PCA complex shown in stereo. **(a)** Amino acid residues completely conserved among the related enzymes are shown in red. The residues from the α subunit are shown in cyan. The substrate PCA (shown in green) makes six hydrogen bonds (dotted lines) with the surrounding amino acid residues. Coordination bonds to the Fe ion are in orange. The putative O_2-binding site (pink arrow) is presumed to be the fourth equatorial ligand in the tetragonal bipyramidal coordination sphere. **(b)** The active site of the BphC–2,3-dihydroxybiphenyl (2,3-DHBP) complex [12] (shown in red) superimposed on that of the LigAB–PCA complex (this study; shown in yellow). The view direction is the same as in (a).

to the vicinal hydroxyl groups of PCA. In, concert with the lift of His12b, His127b is apparently also lifted, resulting in the hydrogen bond between O4 of PCA and Nε of His127b. Seemingly independently, His195b moves rightward, resulting in a weak hydrogen bond between O3 of PCA and Nε of His195b, which may facilitate the role of His195b as the catalytic base (see below). The disruption of the hydrogen-bond network formed by the bound water molecules occupying the PCA-binding cavity and a resultant 'mobilization' of Tyr90a (Figures 8b,c) will be discussed in the next section.

The O_2-binding site

Examining the Fe coordination polyhedron in the PCA complex (Figure 5b and Table 2), we note that the polyhedron is best described as a tetragonal bipyramid. The missing equatorial site must be the binding site for the dioxygen, which must bind to the Fe ion for its activation. A difficulty with this hypothesis is that there is not enough space for accommodating the dioxygen. The required space seems to be occupied by the phenyl sidechain of Tyr90a (Figure 7a). The problematic phenyl group, however, is considerably more flexible than the other sidechains in the active site. Inspection of the surrounding environment indicates that the phenyl group of Tyr90a can easily be rotated around the Cα–Cβ bond to be stored in a cavity located between the α and β subunits. Thus, the presently assumed binding site for dioxygen seems to be sufficiently feasible.

It is intriguing to note that the 'mobile' sidechain of Tyr90a results from the binding of the PCA substrate. As shown in Figure 8b, in the substrate-free state, the Oη of Tyr90a is tightly fixed by hydrogen bonds to two bound

Figure 8

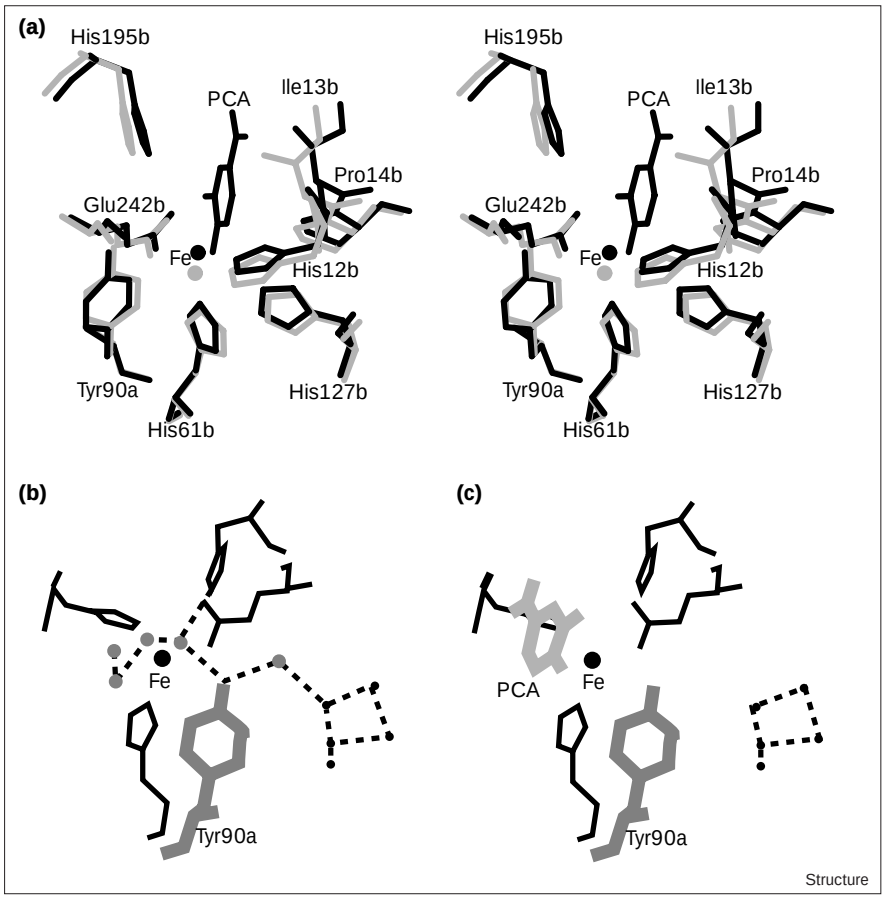

Induced-fit movements around the active site of LigAB upon binding the substrate PCA. (a) The structure of the free enzyme (shown in gray) is superimposed with that of the substrate (PCA) complex (shown in black). In (b) and (c), hydrogen-bonded networks (dotted lines) involving the bound water molecules (shown as gray dots) and Tyr90a (shaded) are shown for the environments (b) before and (c) after binding the substrate PCA (shaded).

water molecules that, in turn, are fixed by a hydrogen-bonded network formed by a set of bound water molecules occupying the cavity reserved for a substrate like PCA. In this state, the average B factor of the Tyr90a phenyl group is 27.4 Å^2. Upon binding PCA, the above-mentioned hydrogen-bonded network is completely disrupted, resulting in an unanchored phenyl group with the average B values being 37.7 Å^2. Thus, the binding of PCA 'mobilizes' the Tyr90a phenyl ring and then the reactive dioxygen can proceed to the Fe center, pushing the mobile phenyl ring aside. In contrast, in the previously analyzed case of BphC [12], the putative O_2-binding site seems to be fixed from the outset and the dioxygen can proceed without further noticable induced-fit movements [12].

Comparison between the BphC and LigAB enzymes

The active sites of the BphC and LigAB enzymes (both as substrate complexes) were superposed with reference to the two hydroxyl groups of the substrates 2,3-DHBP (2,3-dihydroxybiphenyl) in the case of BphC, PCA in the case of LigAB and the Fe ion. Surprisingly, the three proteinaceous coordination sites occupied by two His and one Glu residue superimposed very well (root mean square deviation [rmsd] = 0.21 Å; Figure 7b). In both cases, the axial ligands of the coordination sphere are Nε of a His residue (His209 in BphC, His61b in LigAB) and a hydroxyl group of the substrate. The equatorial ligands are a hydroxyl group of the substrate, Nε of a His residue (His145 in BphC, His12b in LigAB) and Oε of a Glu residue (Glu260 in BphC, Glu242 in LigAB), although the topological manner in which the equatorial sites are occupied by the three ligands is different (Figure 7b). This topological difference might cause a subtle difference in the electronic state of the Fe ion.

Apart from the equatorial topological difference, the coordination spheres and their neighboring environments exhibit a surprising similarity between the two enzyme–substrate complexes. First, the asymmetric hydroxyl binding of the substrate is a common feature in BphC and LigAB. In both cases, two hydroxyl groups of the substrate directly coordinate to the Fe ion, one as an equatorial ligand and the other as an axial one. It is noteworthy that, in both cases, the hydroxyl group attached to one end of the C–C bond to be cleaved (C4–C5 in PCA,

see Figure 1a, and C1–C2 in 2,3–DHBP [12]) is the equatorial ligand. In the LigAB–PCA complex, the equatorially coordinated O4 in PCA seems to be further stabilized by a hydrogen bond with Nε of His127b (2.6 Å). A similar role is played by Oη of Tyr249 in the BphC–2,3-DHBP complex, the distance between Oη and O2 of 2,3-DHBP being 2.7 Å. In the present superposition, the two atoms Nε and Oη deviate by 1.7 Å.

The second striking similarity is related to a putative catalytic base (His195b in LigAB, His194 in BphC). In the case of BphC, it has been pointed out that the imidazole N of His194 must be the catalytic base [15]. This hypothesis was originally set up on the basis of the crystal structure of the BphC–2,3-DHBP complex [12] and the previously proposed reaction mechanism [16,17]. The hypothesis seems to have been sufficiently borne out by many relevant site-directed mutagenesis studies [15]. Now, in the case of the LigAB–PCA complex, the imidazole N of His195b seems to play the same role (Figure 7b). The distance between Nε of His195b and O3 of PCA is 2.9 Å as compared to the corresponding value 3.2 Å; a further refined value (TS, KS, EM, MF and YM, unpublished results) between Nε of His194 and O3 of 2,3-DHBP in the BphC complex.

These common features found around the active sites of BphC and LigAB strongly suggest that they share essentially the same catalytic mechanism despite their completely different polypeptide-chain folding. Despite the striking similarity between the active-site geometries of the LigAB–PCA complex and the BphC–2,3-DHBP complex, the dynamic processes leading to such final structures must be considerably different. The BphC enzyme undergoes only a set of minor and apparently uncoordinated induced-fit movements upon binding substrate [12], whereas the LigAB enzyme undergoes a set of apparently concerted induced-fit movements upon binding PCA (Figure 8a).

As for the binding of a dioxygen (O_2), the difference in dynamic procedures for accommodating it is presumably very large. In the BphC–2,3-DHBP complex, the site for O_2 ligation to the Fe ion seems to be pre-existing [12]. In contrast, in the case of the LigAB–PCA complex, the dioxygen can acquire the space for ligation only after a large scale induced-fit movement of Tyr90a, which is made possible by a mobilization of the phenyl ring as a result of PCA binding (see above).

Biological implications

Catecholic dioxygenases, which cleave the aromatic ring possessing two adjacent hydroxyl substituents with the aid of a molecular dioxygen activated by non-heme iron centers, play an essential role in the metabolic degradation of aromatic compounds in many biological species, especially in aerobic microbes. Such dioxygenases are divided into the intradiol and extradiol types, depending on the location of the cleaved aromatic C–C bond relative to the vicinal hydroxyl groups. The extradiol-type (catecholic) dioxygenases are further divided into classes I, II and III. For class II enzymes, which are the gene-duplication products of class I enzymes, three-dimensional structures have been established. The amino acid sequences of class III enzymes are unrelated to those of class I and II enzymes. This paper is the first report on the three-dimensional structure of a class III enzyme, LigAB (a protocatechuate 4,5-dioxygenase), which is a key enzyme in the lignin-degradation pathway of *Sphingomonas paucimobilis* SYK-6.

Lignin comprises about a quarter of the land-based biomass on earth, and its recycling is vital for the global carbon cycle. The study of the biochemical and enzymatic processes of lignin transformation is expected to supply useful catalytic reactions for the industrial production of valuable chemicals. *S. paucimobilis* SYK-6 can grow on a variety of dimeric lignin compounds, and it is thought to play a role in the bacterial transformation activities responsible for lignin degradation in nature. In this strain, most lignin compounds, including biphenyl compounds, are metabolized to protocatechuate, the ring cleavage of which is catalyzed by a class III enzyme, LigAB. Protocatechuate is metabolized via sequential ring-cleavage and hydrolysis processes analogous to the aerobic biphenyl degradation pathway, in which class II enzymes are involved. It is conceivable that the class II enzymes are evolutionally related to LigAB.

However, the LigAB enzyme structures illustrated in this paper do not exhibit any similarity to those of class II enzymes. Despite the completely unrelated manner of polypeptide chain folding, the active site of LigAB (and other class III enzymes, by inference), centered by a non-heme iron coordination sphere, shares many common geometrical characteristics with those of the class II enzymes, implying that essentially the same reaction mechanism is adopted by the class I, II and III enzymes. Thus, the present comparison between the class II and III extradiol-type (catecholic) dioxygenases provides another clear example of a convergent evolution of two kinds of proteins of distinct ancestry. Finally, the above structural observation would suggest that the lignin-degradation pathway in *S. paucimobilis* SYK-6 has evolved independently from the degradation pathway of biphenyl, although a biphenyl structure is one of the major components of lignin.

Materials and methods

Preparation of crystals

Purification and crystallization of LigAB from *S. paucimobilis* SYK-6 was carried out as described by Sugimoto *et al.* [24]. The crystallization

procedures were carried out in aerobic conditions. The crystals belong to space group $P2_1$ with cell parameters a = 65.4 Å, b = 66.5 Å, c = 119.8 Å, β = 92.5°. An assumption of one LigAB molecule, which has $\alpha_2\beta_2$ subunit composition, per asymmetric unit leads to a Vm value of 2.66 Å^3/Da, corresponding to a solvent content of 53.4%. Crystals of LigAB in complex with its substrate were prepared under aerobic condition by soaking the crystals in the standard buffer (0.1 M Tris/HCl, 60% saturated ammonium sulfate, pH 7.4) containing 10 mM of substrate for 2 h.

Data collection

Diffraction data from the native crystals were collected at room temperature using an R-AXIS IIc (Rigaku) imaging plate area detector with CuKα radiation (generated by Rigaku RU-200 rotating-anode generator operating at 4.95 kW). The data was processed with the software installed on the R-AXIS IIc system.

Diffraction data for derivative crystals were collected at 15°C using a macromolecule-oriented Weissenberg camera devised by N Sakabe [25], installed at BL6A/18B of the 'Photon Factory' synchrotron-radiation source in Tsukuba, Japan. The data was processed using the programs DENZO [26] and SCALA [27].

Structure determination and crystallographic refinement

The crystal structure was solved by an MIR method incorporating anomalous effects for each derivative (Table 1). For crystallographic calculations, the CCP4 program suite [27] was used. Using two heavy-atom derivatives, the phases for 2.5 Å resolution were calculated with the program MLPHARE [27], resulting in a figure of merit of 0.38 (Table 1). The obtained phases were gradually extended up to 2.2 Å resolution using the program DM [27]. In the density-modification procedure, three techniques (histogram matching, solvent flattening and noncrystallographic symmetry (NCS)-averaging) were applied. Structure determination statistics at 2.5 Å resolution are shown in Table 1. Quality of the resultant electron-density map was excellent. Overall chain tracing was carried out without difficulty. The electron-density map was interpreted using the X-ray crystallography applications of the program QUANTA (Molecular Simulation Inc.).

Crystallographic refinement was carried out using the programs X-PLOR [28] and REFMAC [29]. Initially, the program X-PLOR was used, and at the later stage of the refinement, program REFMAC was used. In the course of the crystallographic refinement, free R factors [30] were used to assess the progress of the refinement (a 10% fraction of the whole reflection data was randomly selected and exclusively utilized for calculating the free R factor). The iron coordination sphere was refined without any restraints. Parameter files for PCA were prepared for both the X-PLOR and REFMAC program based on the energy-minimized structure, which was obtained by using the QUANTA/CHARMm system (Molecular Simulation Inc.). One cycle of the crystallographic refinement consisted of one simulated-annealing procedure using X-PLOR, or maximum-likelihood refinement using REFMAC, under noncrystallographic twofold symmetry restraints, followed by model building using QUANTA. In correcting the obtained model, ϕ–ψ plots [31] were used to find the regions with bad geometries. Water molecules were automatically added using the program ARP [32]. The results of the crystallographic refinement are summarized in Table 1.

Tools used for geometrical analyses

The program PROCHECK [33] was used to analyze conformational deviations from the defined norm. All the models derived in the above procedures turned out to have good geometries. The polypeptide chain of the LigAB enzyme, which has an $\alpha_2\beta_2$ subunit composition, has 716 non-glycine and non-proline amino acid residues, all of which are crystallographically independent. Among these, 665 amino acid residues (91.5%) have ϕ, ψ angles within the most favored regions of the Ramachandran plot [31]. Of the remaining 62 residues, 57 (8.0% of the total) have dihedral angles in the additional 'allowed' regions, and two of them (0.3% of the total) have dihedral angles in the 'generously allowed' regions. Two residues (0.3% of the total) had dihedral angles in the 'disallowed' regions of the ϕ–ψ plot. Secondary structural segments were determined using the program PROCHECK [33]. The results are schematically illustrated in Figure 4.

Accession numbers

The coordinates for the LigAB structures have been deposited with the Protein Data Bank with the accession codes 1bou (substrate-free form) and 1b4u (LigAB–PCA complex).

Acknowledgements

We thank T Nonaka for crystallographic discussions. We also thank Yoshihiro Katayama of Graduate school of Bio-Applications and Systems Engineering, Tokyo University of Agriculture and Technology. This study was partly supported by the Promotion of Basic Research Activities for Innovative Bioscience (PROBRAIN) in Japan, the Sakabe project at the TARA (Tsukuba Advanced Research Alliance) center, University of Tsukuba, Japan and Grants-in-Aid for Scientific Research from the Ministry of Education, Science and Culture of Japan, Nos. 10129206, 10490017 given to YM. We acknowledge one of the referees for an important comment on the oxidation state of the Fe ion and related potential conformational change. The other referee is gratefully acknowledged for linguistic corrections.

References

1. Lipscomb, J.D. & Orville, A.M. (1992). Mechanistic aspect of dihyroxybenzote dioxygenase. In *Metal Ions of Biological Systems.* (Sigel, H. & Sigel, A., eds), Vol. 28, pp. 243-298, Marcel Dekker, Inc., New York.
2. Harayama, S., Kok, M. & Neidle, E.L. (1992). Functional and evolutionary relationships among diverse oxygenases. *Annu. Rev. Microbiol.* 46, 565-601.
3. Ohlendorf, D.H., Lipscomb, J.D. & Weber, P.C. (1988). Structure and assembly of protocatechuate 3,4-dioxygenase. *Nature* 336, 403-405.
4. Ohlendorf, D.H., Orville, A.M. & Lipscomb, J.D. (1994). Structure of protocatechuate 3,4-dioxygenase from *Pseudomonas aeruginosa* at 2.15 Å resolution. *J. Mol. Biol.* 244, 586-608.
5. Orville, A.M., Elango, N., Lipscomb, J.D. & Ohlendorf, D.H. (1997). Structure of competitive inhibitor complexes of protocatechuate 3,4-dioxygenase: multiple exogenous ligand binding orientations within the active site. *Biochemistry* 36, 10039-10051.
6. Orville, A.M., Lipscomb, J.D. & Ohlendorf, D.H. (1997). Crystal structure of substrate and substrate analog complexes of protocatechuate 3,4-dioxygenase: endogenous Fe^{3+} ligand displacement in response to substrate binding. *Biochemistry* 36, 10052-10066.
7. Elgren, T.E., Orville, A.M., Kelly, K.A., Lipscomb, J.D., Ohlendorf, D.H. & Que, L. Jr, (1997). Crystal structure and resonance Raman studies of protocatechuate 3,4-dioxygenase complexed with 3,4-dihydroxylphenylacetate. *Biochemistry* 36, 11504-11513.
8. Frazee, R.W., Orville, A.M., Dolbeare, K.B., Yu, H., Ohlendorf, D.H. & Lipscomb, J.D. (1998). The axial tyrosinate Fe^{3+} ligand in protocatechuate 3,4-dioxygenase influences substrate binding and product release: evidence for new reaction cycle intermediates. *Biochemistry* 37, 2131-2144.
9. Spence, E.L., Kawamukai, M., Sanvoisin, J., Braven, H. & Bugg, T.D.H. (1996). Catechol dioxygenase from *Escherichia coli* (MhpB) and *Alcaligenes eutrophus* (MpcI): Sequence analysis and biochemical properties of a third family of extradiol dioxygenase. *J. Bacteriol.* 178, 5249-5256.
10. Eltis, L.D. & Bolin, J.T. (1996). Evolutionary relationship among extradiol dioxygenases. *J. Bacteriol.* 178, 5930-5937.
11. Sugiyama, K., *et al.*, & Mitsui, Y. (1995). Three-dimensional structure of 2,3-dihydroxybiphenyl dioxygenase (BphC enzyme) from *Pseudomonas* sp. strain KKS102 having polychlorinated biphenyl (PCB)-degrading activity. *Proc. Jpn Acad. [B]* 71, 32-35.
12. Senda,T., *et al.*, & Mitsui, Y. (1996). Three-dimensional structures of free form and two substrate complexes of an extradiol ring-cleavage type dioxygenase, the BphC enzyme from *Pseudomonas* sp. strain KKS102. *J. Mol. Biol.* 255, 735-752.
13. Han, S., Eltis, L.D., Timmis, K.N., Muchmore, S.W. & Bolin, J.T. (1995). Crystal structure of the biphenyl-cleaving extradiol dioxygenase from a PCB-degrading Pseudomonad. *Science* 270, 976-980.
14. Kita, A., *et al.*, & Miki, K. (1999). Crystal structure of catechol 2,3-dioxygenase from *Pseudomonas putida* mt-2, metapyrocatechase, an archetypical extradiol-cleaving catecholic dioxygenase. *Structure* 7, 25-34.

15. Senda, T., *et al.*, & Mitsui, Y. (1998). Three-dimensional structure of an extradiol type catechol ring cleavage dioxygenase BphC derived from *Pseudomonas* sp. strain KKS102 – structural feature pertinent to substrate specificity and reaction mechanism. In *Oxygen Homeostasis and its Dynamics*. (Ishimura, Y., Shimada, H. & Suematsu, M. eds), Part 3, pp. 276-281, Springer-Verlag, Tokyo, Japan.
16. Shu, L., Chiou, Y.M., Orville, A.M., Miller, M.A., Lipscomb, J.D. & Que, L. Jr., (1995). X-ray absorption spectroscopic studies of the Fe(II) active site of catechol 2,3-dioxygenase. Implications for the extradiol cleavage mechanism. *Biochemistry* **34**, 6649-6659.
17. Miller, M.A. & Lipscomb, J.D. (1996). Homoprotocatechuate 2,3-dioxygenase from *Brevibacterium fuscum*: a dioxygenase with catalase activity. *J. Biol. Chem.* **271**, 5524-5535.
18. Arciero, D.M., Lipscomb, J.D., Huynh, B.H., Kent, T.A. & Münck, E. (1983). EPR and Mössbauer studies of protocatechuate 4,5-dioxygenase. *J. Biol. Chem.* **258**, 14981-14991.
19. Arciero, D.M., Orville, A.M. & Lipscomb, J.D. (1985). [^{17}O]water and nitric oxide binding by protocatechuate 4,5-dioxygenase and catechol 2,3-dioxygenase. *J. Biol. Chem.* **260**, 14035-14044.
20. Arciero, D.M. & Lipscomb, J.D. (1986). Binding of ^{17}O-labeled substrate and inhibitors to protocatechuate 4,5-dioxygenase-nitrosyl complex. *J. Biol. Chem.* **261**, 2170-2178.
21. Noda, Y., *et. al.*, & Yamasaki, M. (1990). Molecular cloning of the protocatechuate 4,5-dioxygenase genes of *Pseudomonas paucimobilis*. *J. Bacteriol.* **172**, 2704-2709.
22. Murzin, A.G., Brenner, S.E., Hubbard, T. & Chothia, C. (1995). SCOP: A structural classification of proteins database for the investigation of sequences and structures. *J. Mol. Biol.* **247**, 536-540.
23. Luzzati, V. (1952). Traitment statistique des erreurs dans la determination des structures crystallines. *Acta. Crystallogr.* **5**, 802-810.
24. Sugimoto, K., Aoshima, H., Senda, T., Masai, E., Fukuda, M. & Mitsui, Y. (1999). Purification and crystallization of a protocatechuate 4,5–dioxygenase LigAB from *Sphingomonas pausemobilis* SYK-6. *Protein Peptide Lett.* **6**, 55-58.
25. Sakabe, N. (1991). X-ray diffraction data collection system for modern protein crystallography with a Weissenberg camera and an imaging plate using synchrotron radiation. *Nucl. Instrum. Meth. A* **303**, 448-463.
26. Otwinowski, Z. & Minor, W. (1997). Processing of X-ray diffraction Data collected in oscillation mode. *Methods Enzymol.* **276**, 307-326.
27. Collaborative computational project number 4 (1994). The *CCP4 suite: programs for protein crystallography. Acta Crystallogr. D* **50**, 760-763.
28. Brünger, A.T. (1992). *X-PLOR, Version 3.1 Manual*. Yale University Press, New Haven, CT, USA.
29. Murshudov, G.N., Vagin, A.A. & Dodson, E.J. (1997). Refinement of macromolecular structures by the maximum-likelihood method. *Acta Crystallogr. D* **53**, 240-255.
30. Brünger, A.T. (1992). Free R value: a novel statistical quantity for assessing the accuracy of crystal structures. *Nature* **355**, 472-475.
31. Ramachandran, G.N. & Sasisekharan, V. (1968). Conformations of polypeptides and proteins. *Adv. Protein Chem.* **23**, 283-437.
32. Lamzin, V. & Wilson, K.S. (1993). Automated refinement of protein models. *Acta Crystallogr. D* **49**, 129-147.
33. Laskowski, R.A., MacArthur, M.W., Moss, D.S. & Thornton, J.M. (1993). PROCHECK: a program to check the stereochemical quality of protein structures. *J. Appl. Crystallogr.* **26**, 283-291.
34. McRee, D.E. (1993). *Practical Protein Crystallography.* Academic Press, San Diego, CA., USA.
35. Merritt, E.A. & Murphy, E.P. (1994) *Raster3D* Version 2.0. A program for photorealistic molecular graphics. *Acta Crystallogr. D* **50**, 869-873.
36. Kraulis, P. (1991). MOLSCRIPT: A program to produce both detailed and schematic plots of protein structures. *J. Appl. Crystallogr.* **24**, 946-950.
37. Sato, S., Nam, J.W., Kasuga, K., Nojiri, H., Yamane, H. & Omori, T. (1997) Identification and characterization of genes encoding carbazole 1,9a-dioxygenase in *Pseudomonas* sp. strain CA10. *J. Bacteriol.* **179**, 4850-4858.
38. Kabisch, M. & Fortnagel, P. (1990). Nucleotide sequence of metapyrocatechase I (catechol 2,3-oxygenase I) gene *mpcI* from *Alcaligenes eutrophus* JMP222. *Nucleic Acids Res.* **18**, 3405-3406.
39. Barnes, M.R., Duetz, W.A. & Williams, P.A. (1997). A 3-(3-hydroxyphenyl) propionic acid catabolic pathway in *Rhodococcus globerulus* PWD1: Cloning and characterization of the *hpp* operon. *J. Bacteriol.* **179**, 6145-6153.

Because *Structure with Folding & Design* operates a 'Continuous Publication System' for Research Papers, this paper has been published on the internet before being printed (accessed from http://biomednet.com/cbiology/str). For further information, see the explanation on the contents page.